Author(s): Hannonen, Jenna; Kiesilä, Anniina; Mattinen, Ulriika; Pihko, Petri M.; Peljo, Pekka

Title: Electrochemical characterization of redox activity and stability of various tris(2,2'-bipyridine) derived complexes of iron(II) in aqueous solutions

Year: 2023

Version: Published version

Please cite the original version:

Electrochemical characterization of redox activity and stability of various tris(2,2'-bipyridine) derived complexes of iron(II) in aqueous solutions

Jenna Hannonen [a], Anniina Kiesilä [b], Ulriika Mattinen [a], Petri M. Pihko [b], Pekka Peljo [a,c,*]

[a] Research Group of Battery Materials and Technologies, Department of Mechanical and Materials Engineering, University of Turku, FI-20014 Turun yliopisto, Finland
[b] Nanoscience Center and Department of Chemistry, University of Jyväskylä, FI-40014 Jyväskylän yliopisto, Finland
[c] Department of Chemistry and Materials Science, Aalto University, FI-00076 Aalto, Finland

ARTICLE INFO

ABSTRACT

Tris(2,2'-bipyridine) Fe(II) complexes with different 4,4'-placed substituents were studied electrochemically in aqueous solutions. Digital simulation of the experimental cyclic voltammograms enabled the evaluation of the redox potentials, electrochemical kinetics as well as complex stability. The substituent effect on the formal potential of the complexes was investigated, showing that electron-withdrawing substituents shift the formal potential to a positive direction from the potential of the unsubstituted $[Fe(II)(bpy)_3]^{2+}$ complex (0.875 V $vs.$ Ag/AgCl). Respectively electron-donating substituents shift the formal potential to a negative direction. The most positive formal potential (0.97 V $vs.$ Ag/AgCl) was obtained with 4,4'-dicarboxyl substituted and the lowest 0.56 V $vs.$ Ag/AgCl with 4,4'-di-OMe substituted $[Fe(II)(bpy)_3]^{2+}$. We show here that the stability of the compounds in the oxidized form can be evaluated by voltammetry. None of the studied complexes was stable enough for flow battery applications, but knowledge of their decomposition rates was obtained via simulations, considering that all oxidized species undergo a chemical reaction, resulting in a loss of redox-active species. The counterion of the complex affected the solubility and stability of the complex, as the presence of tetrafluoroborate resulted in faster decomposition than the presence of sulfate. Battery testing of the most stable Fe(II) complex revealed a voltage drop upon discharge, lowering the energy efficiency. Battery cycling showed a capacity decay most likely related to the chemical reaction occurring to the oxidized species. Even though the studied complexes are not suitable for aqueous flow battery applications as such, knowledge of a substituent, counterion, and electrolyte effect on their performance is needed to develop these complexes further and to improve their stability via structural design. We show here that voltammetry is a suitable tool for fast initial evaluation of the stability of the materials.

1. Introduction

2,2'-Bipyridine (bpy) was first synthesized already in 1888[1] and is one of the widely utilized ligands[2] complexing a variety of metals. The coordination chemistry of 2,2'-bipyridine was defined 10 years later[3], when $[Fe(II)(bpy)_3]^{2+}$ with 3:1 ratio of bpy and iron was synthesized and described. In the same work the oxidation of this complex into $[Fe(III)(bpy)_3]^{3+}$ was described. The redox ability of Fe(II) compounds was discovered in 1931[4], activating interest in their electrochemical research. Since then, metal complexes with 2,2'-bipyridine as ligands have been tested for different electrochemical applications. First study [5] of the bpy-metal complexes for flow battery applications was initiated with $[Ru(II)(bpy)_3]^{2+}$ stating back to 1988. Recently, also other

metals have been complexed with 2,2'-bipyridine and bipyridine-based ligands, like 1,10-phenanthroline, and studied as a possible redox active species in flow batteries.[6–10] As iron bipyridine complexes have very positive redox potentials, we were interested to evaluate their suitability as positive electrolytes for aqueous flow batteries.

When developing active materials for flow batteries, it is important to obtain a sufficiently high cell potential, without compromising the stability. It is well known that ligands can significantly affect the redox potentials of metals. For example, the redox potential of Fe^{3+}/Fe^{2+} redox couple shifts by ca. + 0.3 V from + 0.77 V $vs.$ SHE to + 1.03 V $vs.$ SHE when complexed with bipyridine, and by –0.32 V down to 0.358 V $vs.$ SHE when complexed with cyanide.[11] This large variability allows tuning of the redox potentials of the metal complexes by changing the

* Corresponding author at: Research Group of Battery Materials and Technologies, Department of Mechanical and Materials Engineering, University of Turku, FI-20014 Turun yliopisto, Finland.
E-mail address: pekka.peljo@utu.fi (P. Peljo).

ligands in the complex, and tuning the structure of the ligands with substituents. The adjustability of the redox potential makes metal complexes attractive as candidates for redox active materials for flow batteries, regardless of their rather large molecular mass per the stored electrons.

There is a growing interest to use iron complexed with different organic ligands in flow batteries due to the cost-efficiency, sustainability, and electrochemical performance required from energy storage materials. Currently, ferrocyanide is a popular choice as a positive electrolyte for flow batteries operating at neutral or alkaline pH. However, its redox potential is rather low and new candidates for the positive electrolyte improving the cell potential of the flow battery should be found.

Tuning the structure of a complex with ligands with different substituents affects the solubility and stability of the complex. Solubility is also affected by the counterions balancing the charge of the complex. Recently, the stability and solubility of an iron complex were improved by introducing an asymmetric ligand design for $M_4[Fe(II)(Dcbpy)_2(CN)_2]$ (M = Na, K) complex, cycled as a positive electrolyte showing good performance. Dcbpy denotes 4,4'-dicarboxyl-2,2'-bpy [12]. The solubility of this complex was affected by the choice of the counterion (Na^+, K^+) for the complex. Asymmetric complexes and molecules have in general a better solubility than symmetric complexes according to Carnelley's rule[13].

The stability of the Fe(II) complexes in the solution can be followed by observing solid precipitate formation and changes in the colour of the solution over time. Stability for Fe(III) species can be obtained via simulations of cyclic voltammograms (CVs) via the presence of an EC reaction[14]. EC reaction indicates a following chemical reaction (C) taking place in the solution after the electron transfer (E). Thus, during the cyclic voltammetry measurements, the amount of redox-active species decreases upon oxidation. This can be seen as the difference between oxidation and reduction currents in CVs, as they would be equal in a reversible case without the following chemical reaction. Voltammograms can be simulated digitally by considering diffusion with Fick's second law for redox species and implementing an EC reaction scheme by considering the loss of redox-active species at a certain rate. These formulae are presented in detail in the model description in the electronic supplementary information (ESI). In this work, we used COMSOL Multiphysics software for simulations to obtain qualitative information about the kinetics of the redox species and the rate of the chemical reaction following the oxidation to compare the stabilities of different Fe(III) species in near neutral pH aqueous electrolytes.

Most of the current investigations on the use of iron bipyridine complexes in flow batteries are done in non-aqueous media and ionic liquids. Redox potentials of $[Fe(II)(bpy)_3]^{2+}$ complexes have been studied in organic solutions with different substituents, while a

systematic study of their redox potentials and stabilities has not been conducted in water solutions before. Therefore, the electrochemical properties of a series of iron bipyridine complexes were measured in an aqueous solution of 0.1 M phosphate buffer (pH 7). This series consisted of tris(4,4'-di-R-2,2'-bpy)Fe(II) complexes without a substituent (R) and with substituents of Me, *t*Bu, OMe, CO_2Me, COO^- or Br, with sulfate (SO_4^{2-}) or tetrafluoroborates (BF_4^-) as counterions. Complexes will be referred to as $[Fe(II)(DR-bpy)_3]^{2+}$, where DR denotes di-4,4'-placed substituents as explained previously and demonstrated in Fig. 1. Exception to the positively charged Fe(II) complexes is $Na_{4+x}[Fe(II)(Dcbpy)_3](BF_4)_x$ with negatively charged 4,4'-dicarboxyl-2,2'-bpy ligands, hence resulting in a negatively charged $[Fe(II)(Dcbpy)_3]^{4-}$. The complexes with sulfate counterion were investigated further in 0.1 M KNO_3, 0.1 M K_2SO_4 and 0.1 M NaCl water solutions. Additionally, we studied tris(2,2'-bipyrazine)Fe(II)$(BF_4)_2$, with tetrafluoroborate counterions in 0.1 M phosphate buffer (pH 7) and this complex will be referred to as $[Fe(II)(bpz)_3](BF_4)_2$. The general structures of the studied complexes are presented in Fig. 1.

Cyclic voltammetry measurements show that most of the synthesized Fe(II) complexes undergo an electrochemical oxidation to Fe(III) followed by an irreversible chemical reaction. Digital simulations of the electrochemical response allow extraction of both the standard rate constant (k^0) of the electrochemical reaction as well as the rate constant of the following chemical reaction (k_c). Electrochemical stability of the iron complexes was also studied by cycling a lab-scale flow battery. Battery testing was performed in an asymmetric as well as in a symmetric battery set-up, to evaluate the capacity decay and to monitor the change in the shape of the charge–discharge responses. Although none of the complexes investigated in this study show sufficient stability for aqueous flow battery applications as such, understanding the stability of the metal complexes is valuable for developing more stable bipyridine-based compounds. Improved stability may be achieved by asymmetric ligand design, like in a recently reported[12] iron complex with Dcbpy and cyanide ligands. Another possible way to stabilize the metal complex structure is to find a suitable sidegroup to the ligand, like in a recently reported[15] tris(4,4'-bis(hydroxymethyl)-2,2'-bipyridine) iron(II) dichloride utilized as a posolyte at near-neutral pH resulting in high positive potential and low capacity decay in an aqueous flow battery.

2. Experimental

2.1. Synthetic procedures

The respective bipyridine ligand was dissolved in a minimal amount of ethanol, methanol, water or acetonitrile depending on their solubility. $FeSO_4 \cdot 7H_2O$ was dissolved to a minimal amount of H_2O and Fe
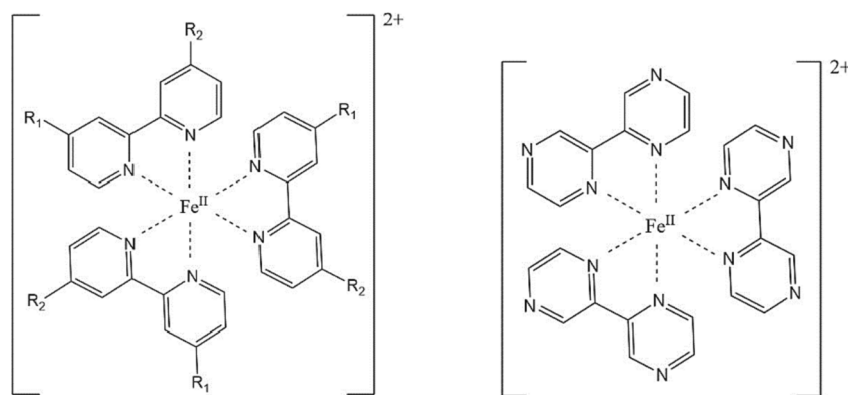

Fig. 1. General structures of the studied Fe complexes presented in the dissolved reduced state, with a total charge of 2+ with neutral sidegroups. Counterions in the solid form can be either a single SO_4^{2-} ion or two BF_4^- ions per complex. With negatively charged Dcbpy ligands, the complex is negatively charged $[Fe(II)(Dcbpy)_3]^{4-}$, having Na^+ and BF_4^- as counterions in the solid structure. In the water solutions, the counterions are dissolved and thus further away from the complexes. On the left: $[Fe(II)(bpy)_3]^{2+}$ with neutral sidechains of R_1 and R_2. On the right: $[Fe(II)(bpz)_3]^{2+}$.

$(BF_4)_2 \cdot 6H_2O$ to a minimal amount of MeOH. The ligand (3 eq) and salt (1 eq) were mixed, and the deep red-colored solution was refluxed. The solution was cooled to room temperature and filtered if needed. The filtrate was concentrated under reduced pressure. Yields were near quantitative. Synthesis of the $Na_{4+x}[Fe(II)(Dcbpy)_3](BF_4)_x$ is described in the ESI.

2.2. Characterization

NMR spectra were measured with Bruker Avance 300, 400 and 500 MHz instruments at 303 K. Carbon chemical shifts in D_2O were calibrated by adding a drop of methanol to the sample. The signal was defined as 49.50 ppm.[16] ^{19}F measurements were calibrated using external reference C_6H_5F (-113.15 ppm). High-resolution mass spectrometry measurements were performed with Micromass LCT ESI-TOF-MS instrument by using a lock-mass method. Theoretical *m/z* values were calculated using chemcalc (chemcalc.org).[17] IR was measured with Bruker Tensor 27 FTIR spectrometer. Melting points were determined with Stuart Scientific Melting point apparatus SMP3.

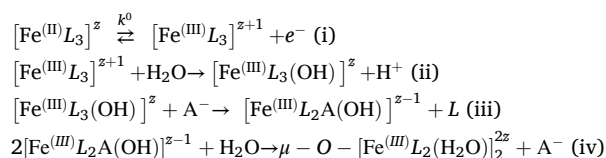### 2.3. Electrochemical measurements

Iron complex concentration used in the CV measurements was 0.5–0.6 mM in the respective electrolyte solution. All samples were measured in a self-prepared 0.1 M sodium phosphate buffer solution (pH 7), and some of the complexes were also measured in 1 M sulfuric acid solution. Complexes with sulfate counterion were further tested in aqueous 0.1 M KNO_3, 0.1 M K_2SO_4 and 0.1 M NaCl solutions. $Na_{4+x}[Fe(II)(Dcbpy)_3](BF_4)_x$ was further investigated in potassium hydrogen phthalate buffer (pH 4.01, Merck KGaA), in 0.5 M NaCl solution as well as in acidic media (0.5 M NaCl and HCl mixture, pH 2.4). The structure chosen to calculate the concentration of $Na_{4+x}[Fe(II)(Dcbpy)_3](BF_4)_x$ for the electrochemical measurements and digital simulations was $Na_6[Fe(II)(Dcbpy)_3](BF_4)_2$, which may be a potential source of uncertainty compared to the real concentration.

Cyclic voltammetry measurements were performed in a three-electrode cell to determine the redox potentials of the samples by using Gamry Reference 600+ potentiostat. Glassy carbon (3 mm diameter, BASi) was used as a working electrode, a commercial Ag/AgCl electrode (3 M KCl, BASi) as a reference electrode, and a platinum wire as a counter electrode. Ohmic resistances of the solutions in a three-electrode cell were evaluated with electrochemical impedance spectroscopy at high frequency. All iron complex solutions were stored after the CV measurements, and their color change and solid precipitate formation were observed over time to compare their chemical stability in glass vials in ambient conditions.

Battery testing was performed with a battery cycler (LANHE Battery Testing System G340A) with a 5 cm^2 lab-scale flow battery cell consisting of graphite current collectors, carbon felt electrodes (thickness 4.6 mm, thermally activated, SGL), and a DSVN membrane (anion-exchange membrane, Selemion). The flow rate in all battery tests was 50 ml/min. $[Fe(II)(DMe-bpy)_3]SO_4$ was studied as a posolyte in a lab-scale flow battery in 0.1 M K_2SO_4 in an asymmetric cell having NDI (naphthalene-diimide)[18] as a negolyte to observe the shape of the charge/discharge curve. This Fe(II) complex was also tested as a posolyte in 0.1 M K_2SO_4 in a symmetric cell having the charged (oxidized) Fe(II) complex, $[Fe(III)(DMe-bpy)_3]^{3+}$, in 0.1 M K_2SO_4 as the negolyte. This negolyte was prepared by oxidizing the Fe(II) species first in a separate battery cell and then transferring the Fe(III) solution to the symmetric battery to be tested as a negolyte against the $[Fe(II)(DMe-bpy)_3]SO_4$ as the posolyte. This way we were able to study if the capacity decay of the asymmetric battery originated from the instability of the Fe(II) and Fe(III) species of the $[Fe(II)(DMe-bpy)_3]SO_4$ complex.

2.4. Finite element method simulations of electrochemical response

The oxidation of the Fe(II) complex to the Fe(III) (eq. i) can result in the decomposition of the oxidized species via chemical reaction by a loss of the ligand (eq. iii) to form a different Fe(III) species, as discussed by Chen et al.[19] Holubowitch et al[20] reported that with the $[Fe(III)(bpy)_3]^{3+}$ the reaction sequence proceeds in four steps: i) redox reaction, ii) nucleophilic attack by a water molecule, iii) a loss of a bpy ligand, iv) dimerization. We describe this as the general following chemical reaction.

$$\left[Fe^{(II)}L_3\right]^z \underset{}{\overset{k^0}{\rightleftharpoons}} \left[Fe^{(III)}L_3\right]^{z+1} + e^- \text{ (i)}$$
$$\left[Fe^{(III)}L_3\right]^{z+1} + H_2O \rightarrow \left[Fe^{(III)}L_3(OH)\right]^z + H^+ \text{ (ii)}$$
$$\left[Fe^{(III)}L_3(OH)\right]^z + A^- \rightarrow \left[Fe^{(III)}L_2A(OH)\right]^{z-1} + L \text{ (iii)}$$
$$2[Fe^{(III)}L_2A(OH)]^{z-1} + H_2O \rightarrow \mu - O - [Fe^{(III)}L_2(H_2O)]_2^{2z} + A^- \text{ (iv)}$$

where L represents the ligand, A^- is the anion and k^0 is the standard rate constant of the electrochemical reaction. The charge of the complex *z* depends on the charge of the ligand. For neutral bipyridine, z = +2. We consider that k_c is the rate of the rate limiting step of the following chemical reaction sequence. The rate limiting step is most probably a first order reaction. Holubowitch et al[20] did not report the energy-barriers for the mentioned reaction steps, but they reported the Gibbs energies dropping the least between the products of the nucleophilic attack and the ligand dissociation. First-order reaction as the ligand dissociation is, is considered to be a common decomposition mechanism for complexes and therefore a first order reaction is used in the simulations to determine the chemical reaction.

The loss of oxidized species via chemical reaction is visible in the current responses for the oxidation and reduction reactions in the experimental CVs. Parameters describing the electron transfer process and the following chemical reaction, such as the rate for the chemical reaction k_c, diffusion coefficient *D*, standard rate constant for the electrochemical reaction k^0 and charge transfer coefficient α, can be extracted from the digital simulations of the system via the commercial COMSOL Multiphysics software by utilizing the finite element method to solve the model. Each voltammogram was fitted separately. The parameters were extracted by adjusting the peak placement of the simulated CV by altering the k^0 value, after which the oxidation peak current was fitted by adjusting the value of *D*. Lastly, the reduction peak current was matched to the experimental by adjusting the value of k_c. α was taken as 0.5. Differences of the peak potentials and peak currents for the forward and reverse sweeps were considered as figures of merit. Based on the sensitivity studies of the obtained parameters the uncertainty of the *D* is below 10 %. For high (0.070 1/s) k_c values the uncertainty is similar but increases with the lower value of k_c. The uncertainty of the k^0 is of ca. 50 % for values within 10^{-3}–10^{-2} cm/s. These uncertainty studies are shown in the ESI, together with the detailed model description.

3. Results and discussion

3.1. Electrochemical measurements

Selected examples of voltammograms of 0.5 mM samples of the synthesized complexes in 100 mM phosphate buffer, pH 7, are shown in Fig. 2. The formal potentials E^0 of the redox pairs were taken as the average of the peak potentials for oxidation and reduction, yielding a half-wave potential approximated to be the formal potential as in equilibrium, and are presented in Table 1 for every measured sample. Complexes were synthesized with two different counterions (sulfate or
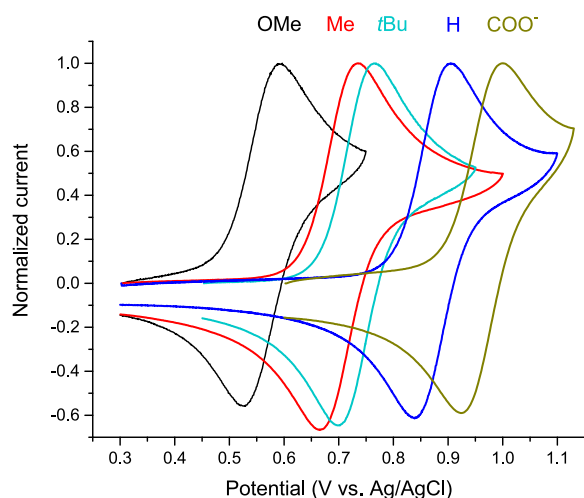
Fig. 2. Normalized CVs of $[Fe(II)(DR\text{-bpy})_3]^{2+}$ show the effect of the substituent (R) on the formal potential. R = H represents the unsubstituted $[Fe(II)(bpy)_3]^{2+}$ complex. Normalization was performed by leveling all CVs to start from zero current, after which all current values were divided with the peak current of oxidation. The scan rate was 100 mV/s.

tetrafluoroborate). As expected, the counterions did not affect the redox potentials. It is worth noting that the sulfate or tetrafluoroborate concentration (0.5 mM, 1 mM) is very small compared to the medium (100 mM). Most complexes were soluble in phosphate buffer in the applied 0.5 mM concentration, except for $[Fe(II)(DtBu\text{-bpy})_3](BF_4)_2$ that was measured in a saturated lower concentration due to poor solubility. The CVs with different scan rates of all the measured samples in different electrolytes are found in ESI.

The Fe^{2+}/Fe^{3+} redox pair on the positive potential range is visible in the CVs for all of the complexes except for $[Fe(II)(D(CO_2Me)\text{-bpy})_3](BF_4)_2$, $[Fe(II)(DBr\text{-bpy})_3](BF_4)_2$ and $[Fe(II)(bpz)_3](BF_4)_2$. The CV of $[Fe(II)(D(CO_2Me)\text{-bpy})_3](BF_4)_2$ showed two redox pairs at -0.95 V and -0.189 V $vs.$ Ag/AgCl, suggesting that the structure of the measured

complex might differ from the assumed structure. The redox pair at -0.95 V showed a double peak for oxidation, which started merging into one peak at increased scan rates. In a non-aqueous solution, the reported E^0 value for $Fe(D(CO_2Me)\text{-bpy})_3(BF_4)_2$ is 1.53 V $vs.$ Ag/AgCl.[21] $[Fe(II)(DBr\text{-bpy})_3](BF_4)_2$ decomposed quickly, even before we could measure it electrochemically, indicating instability in a water solution, since an E^0 value of 1.43 V $vs.$ Ag/AgCl has been reported[20] in a non-aqueous solution. $[Fe(II)(bpz)_3](BF_4)_2$ lost its color soon after dissolving, indicating instability in the water solution.

3.1.1. Redox potentials

The influence of the ligand substituent on the redox potential of the Fe(II) complex is shown in Fig. 2 and Table 1. A clear trend on how the substituents of the bipyridine ligand affect the redox potential of the Fe (II) complex can be seen. Electron withdrawing groups in $Na_{4+x}[Fe(II)(Dcbpy)_3](BF_4)_x$ make the redox potential more positive than for $[Fe(II)(bpy)_3]^{2+}$ by drawing electrons towards themselves from the bpy ligand, hence making the environment of the Fe(II) ion more positive. The larger positive charge of the environment hampers the oxidation of the Fe(II), resulting in an increased oxidation potential compared to $[Fe(II)(bpy)_3]^{2+}$ with the smaller positive charge around the Fe(II) center. Electron donating sidegroups (Me, tBu and OMe) in bpy ligands lead to lower redox potentials of the complex than with $[Fe(II)(bpy)_3]^{2+}$ by pushing electrons towards the Fe center and therefore adding electron density near the Fe(II) ion. This makes the oxidation of the Fe(II) ion easier, as expelling the excess negative charge via oxidation is favorable. It can also be seen that a complex with a stronger electron-donating substituent (OMe) has a smaller oxidation potential than a complex with weaker electron donor sidegroups (Me and tBu). Fe(II) complexes with Me and tBu sidegroups show a small difference in redox potentials. Me group shifts the E^0 value more to negative direction than tBu, indicating the electron density of the Fe(II) ion is less positive due to the Me substituent.

Redox potentials of the typical $[Fe(II)(bpy)_3]^{2+}$ complexes are in the range of 0.56–0.97 V $vs.$ Ag/AgCl. The most positive redox potential was achieved for $Na_{4+x}[Fe(II)(Dcbpy)_3](BF_4)_x$ with the electron-withdrawing dicarboxyl substituent in the $[Fe(II)(bpy)_3]^{2+}$ structure.

Table 1

Measured formal potentials E^0 and solution resistances of the iron complexes in phosphate buffer pH 7. *Due to small shifts in peak placements, the formal potential is given based on scan rate 100 mV/s. **Values for this complex in pH 4: E^0 $vs.$ Ag/AgCl = 0.963 V, $R = 314\ \Omega$. n/a = data not available due to decomposition before CV measurement.

Complex	Counterion	E^0 $vs.$ Ag/AgCl	E^0 $vs.$ SHE	Solution resistance R	Reported E^0 values, electrolyte and reference
$[Fe(II)(bpy)_3]^{2+}$	SO_4^{2-}	0.875 V	1.080 V	144 Ω	0.84 V $vs.$ Ag/AgCl, 1 M NaCl, [21] 0.87 V $vs.$ Ag/AgCl, 1 M IPA [21]
	BF_4^-	0.872 V	1.077 V	144 Ω	1.25 V $vs.$ Ag/AgCl, 0.5 M TEABF$_4$ in propylene carbonate (dry) [20]
	$[ClO_4]^-$				0.682 V $vs.$ Ag/Ag$^+$ (0.010 M AgNO$_3$ in CH$_3$CN), 0.1 M TBAPF$_6$ in AcN [22]
$[Fe(II)(DMe\text{-bpy})_3]^{2+}$	SO_4^{2-}	0.705 V	0.910 V	153 Ω	
	BF_4^-	0.700 V	0.905 V	153 Ω	1.07 V $vs.$ Ag/AgCl, 0.5 M TEABF$_4$ in propylene carbonate (dry) [20]
	$[ClO_4]^-$				0.523 V $vs.$ Ag/Ag$^+$ (0.010 M AgNO$_3$ in CH$_3$CN), 0.1 M TBAPF$_6$ in AcN [22]
$[Fe(II)(DtBu\text{-bpy})_3]^{2+}$	SO_4^{2-}	0.725 V	0.930 V	167 Ω	
	BF_4^-	0.729 V*	0.934 V	130 Ω	1.09 V $vs.$ Ag/AgCl, 0.5 M TEABF$_4$ in propylene carbonate (dry) [20]
$[Fe(II)(D(OMe)\text{-bpy})_3]^{2+}$	SO_4^{2-}	0.560 V	0.765 V	143 Ω	
	BF_4^-	0.560 V	0.765 V	152 Ω	0.94 V $vs.$ Ag/AgCl, 0.5 M TEABF$_4$ in propylene carbonate (dry), [20]
	$[ClO_4]^-$				0.363 V $vs.$ Ag/Ag$^+$ (0.010 M AgNO$_3$ in CH$_3$CN), 0.1 M TBAPF$_6$ in AcN [22]
$[Fe(II)(D(CO_2Me)\text{-bpy})_3]^{2+}$	BF_4^-	-0.950 V*; -0.189 V*	-0.745 V; 0.016 V	146 Ω	1.53 V $vs.$ AgCl in TEABF$_4$/PC (0.5 M) [20]
$[Fe(II)(DBr\text{-bpy})_3]^{2+}$	BF_4^-	n/a	n/a	n/a	1.43 V $vs.$ AgCl in TEABF$_4$/PC (0.5 M) [20]
$Na_{4+x}[Fe(II)(Dcbpy)_3](BF_4)_x$ **	BF_4^-	0.970 V	1.175 V	157 Ω	0.95 V $vs.$ Ag/AgCl in 0.5 M NaCl (aq). Complex is $Na_4[Fe(II)(Dcbpy)_3]$. [12]
$[Fe(II)(bpz)_3](BF_4)_2$	BF_4^-	n/a	n/a	n/a	

However, its redox potential may be too positive for flow battery applications, since it is very close to the onset of the oxygen evolution observed at ca. 1.1 V *vs.* Ag/AgCl. Additionally, irreversible oxidation of the Dcbpy ligand has been reported to be at ca. 1.1 V *vs.* Ag/AgCl.[12] The thermodynamic potential for oxygen evolution in pH 7 is ca. 0.82 V *vs.* SHE, or 0.62 V *vs.* Ag/AgCl, so only OMe substituted iron(II) bipyridine complex would be within the thermodynamic stability window of water at pH 7. In practice, sluggish kinetics of oxygen evolution reaction on carbon electrode shift the stability window to more positive values. Thus, electron-withdrawing groups that can adjust the redox potential of the Fe complex within the kinetic limitations set by water are needed.

Our measured redox potentials agree with earlier studies in the literature[12,21–23] (Table 1.). The reported E^0 values of similar iron complexes have different values than ours due to different solvents, but the nature of the sidegroup affects the redox potentials according to the electron-withdrawing or electron-donating nature of the substituent, as we described above. The differences between the redox potentials of the iron complexes in the aqueous solutions are of same magnitude with the corresponding potentials in the organic solution. For example the difference in redox potentials between $[Fe(II)(DMe\text{-}bpy)_3]^{2+}$ and $[Fe(II)(DtBu\text{-}bpy)_3]^{2+}$ differ by ca. 20 mV both in phosphate buffer (aqueous) and in 0.5 M $TEABF_4$ in propylene carbonate (dry) (organic).

Counterions in the structures do not affect the redox potential of the compounds but they do affect indirectly the electrochemical performance via solubility. Poor solubility limits the suitability of some of the studied compounds for flow batteries. Comprehensive solubility tests

were not made. The concentration applied was very low (0.5 mM) and not all complexes with tetrafluoroborate counterions were soluble to that extent. Solubility can be improved by selecting optimal counterions and supporting electrolyte[12], asymmetric ligand design[12], or by functionalizing the bipyridine with solubilizing groups such as charged or hydrogen bonding groups. For example, $[Fe(II)(bpy)_3]^{2+}$ with COOH functionalization ($M_4[Fe(II)(Dcbpy)_3]$, M = Na, K), has been reported [12] to show a solubility of 0.26 M and 0.6 M in water, with sodium and potassium ions in their structure respectively. In the same work, asymmetric ligand design increased the solubility with a factor of 4.2 to 1.22 M, by replacing a bipyridine with 2 cyanide groups to form $M_4[Fe(II)(Dcbpy)_2(CN)_2]$.

3.2. Electrochemical simulations

Electrochemical simulations were performed with COMSOL Multiphysics software to obtain information about the diffusion and kinetics of the Fe^{3+}/Fe^{2+} redox couple in various $[Fe(II)(bpy)_3]^{2+}$ complexes. The computational CVs were fitted to the experimental CVs of the complexes measured in different aqueous electrolytes: 0.1 M phosphate buffer (pH 7), 0.1 M KNO_3, 0.1 M K_2SO_4 and 0.1 M NaCl. The simulated CVs were individually fitted to the experimental CVs per scan rate, and the average values are reported for most complexes. For some, the 10 mV/s was excluded due to obtaining a better common fit for all scan rates. The resulting CVs are shown in ESI for every simulation and compared to the experimental CVs. The best fitting values for all scan

Table 2

Electrochemical parameters extracted from the digital simulations of the experimental data in phosphate buffer. RSD is given in brackets after each value to represent the ratio of standard deviation *vs* the used fitting parameter. *in phthalate buffer, pH 4 **simulated based on data reported in ref 12. More information is in ESI with experimental and simulated CVs, parameter values per scan rate and the standard deviations.

Complex and counterion	$D \times 10^6$ [cm²/s]	$k^0 \times 10^2$ [cm/s]	α	k_c [1/s]
$[Fe(II)(bpy)_3]SO_4$	1.90 (16.5 %)	1.13 (61.7 %)	0.5	0.017 (7.1 %)
$[Fe(II)(bpy)_3](BF_4)_2$	1.89 (5.8 %)	3.16 (84.6 %)	0.5	0.045 (18.6 %)
$[Fe(II)(DMe\text{-}bpy)_3]SO_4$	0.85 (3.7 %)	1.18 (50.3 %)	0.5	0.009 (5.3 %)
$[Fe(II)(DMe\text{-}bpy)_3](BF_4)_2$	2.32 (6.7 %)	1.28 (45.8 %)	0.5	0.020 (48.8 %)
$[Fe(II)(DtBu\text{-}bpy)_3]SO_4$	1.28 (8.2 %)	1.05 (54.0 %)	0.5	0.016 (56.0 %)
$[Fe(II)(DtBu\text{-}bpy)_3](BF_4)_2$	0.39 (12.9 %)	0.35 (40.2 %)	0.5	0.059 (53.5 %)
$[Fe(II)(D(OMe)\text{-}bpy)_3]SO_4$	0.66 (7.8 %)	1.12 (37.2 %)	0.5	0.075 (21.3 %)
$[Fe(II)(D(OMe)\text{-}bpy)_3](BF_4)_2$	0.12 (6.0 %)	0.49 (42.0 %)	0.5	0.048 (16.3 %)
$Na_{4+x}[Fe(II)(Dcbpy)_3](BF_4)_x$	0.38 (7.9 %)	0.05 (0 %)	0.3	0.158 (62.7 %)
$Na_{4+x}[Fe(II)(Dcbpy)_3](BF_4)_x$*	0.59 (2.9 %)	0.44 (25.0 %)	0.5	0.015 (66.1 %)
$Na_4[Fe(II)(Dcbpy)_3]$ **	2.30	0.40	0.5	0.000

Table 3

Electrochemical parameters extracted from the digital simulations of the experimental data of Fe(II) complexes with sulfate counterions in different electrolytes. Relative standard deviation is given in brackets after each value to represent the ratio of standard deviation *vs* the used fitting parameter in percentage (%). More information is found in ESI with experimental and simulated CVs, parameter values per scan rate and the standard deviations.

Complex and electrolyte	$D \times 10^6$ [cm²/s]	$k^0 \times 10^2$ [cm/s]	α	k_c [1/s]
$[Fe(II)(bpy)_3] SO_4$				
0.1 M phosphate buffer pH 7	1.90 (16.5 %)	1.13 (61.7 %)	0.5	0.017 (7.1 %)
0.1 M KNO_3	3.03 (2.2 %)	2.51 (63.1 %)	0.5	0.006 (61.2 %)
0.1 M K_2SO_4	2.73 (2.8 %)	2.02 (53.5 %)	0.5	0.010 (8.8 %)
0.1 M NaCl	2.89 (0.6 %)	2.26 (44.9 %)	0.5	0.003 (14.3 %)
$[Fe(II)(DMe\text{-}bpy)_3] SO_4$				
0.1 M phosphate buffer pH 7	0.85 (3.7 %)	1.18 (50.2 %)	0.5	0.009 (5.3 %)
0.1 M KNO_3	1.7 (1.6 %)	2.12 (61.0 %)	0.5	0.003 (20.5 %)
0.1 M K_2SO_4	1.32 (2.4 %)	1.97 (52.5 %)	0.5	0.002 (99.1 %)
0.1 M NaCl	1.35 (2.5 %)	2.46 (63.5 %)	0.5	0.002 (83.6 %)
$[Fe(II)(DtBu\text{-}bpy)_3] SO_4$				
0.1 M phosphate buffer pH 7	1.28 (8.2 %)	1.05 (54.0 %)	0.5	0.016 (56.0 %)
0.1 M KNO_3	n/a	n/a	n/a	n/a
0.1 M K_2SO_4	1.92 (2.6 %)	1.44 (42.6 %)	0.5	0.014 (55.7 %)
0.1 M NaCl	1.82 (3.4 %)	2.69 (63.8 %)	0.5	0.009 (77.2 %)
$[Fe(II)(D(OMe)\text{-}bpy)_3] SO_4$				
0.1 M phosphate buffer pH 7	0.66 (7.8 %)	1.12 (37.2 %)	0.5	0.075 (21.3 %)
0.1 M KNO_3	1.77 (10.8 %)	1.67 (40.9 %)	0.5	0.024 (36.1 %)
0.1 M K_2SO_4	1.42 (2.3 %)	4.08 (54.2 %)	0.5	0.028 (28.2 %)
0.1 M NaCl	1.68 (4.9 %)	3.97 (56.2 %)	0.5	0.030 (31.9 %)

rates for diffusion coefficient (D), charge transfer coefficient (α) and reaction rates for both the redox process (k^0) and the following chemical reaction (k_c) in phosphate buffer were determined and are presented in Table 2 for each simulated complex. Results of the simulations for Fe(II) complexes with sulfate counterions in different electrolytes are presented in Table 3. When possible, the charge transfer coefficient was adjusted to be close to 0.5 as expected for typical electrochemical reactions.[14] Resistances of the solutions and the real concentrations of the complexes were considered in the simulations. Difficulty in defining the exact molar mass of $Na_{4+x}[Fe(II)(Dcbpy)_3](BF_4)_x$ complex is a potential source of uncertainty. The concentration of the complex was calculated based on the molar mass of $Na_6[Fe(II)(Dcbpy)_3](BF_4)_2$, leading to a possible deviation in the digital simulations of this complex.

For all complexes, the rising of the current in the forward scan after the oxidation peak causes possible deviation to the simulation results. A great amount of this current was observed for the $Na_{4+x}[Fe(II)(Dcbpy)_3]$ $(BF_4)_x$ complex and can be explained by the partly overlapping oxidation peak of the ligand ($E_{ox} = ca.$ 1.1 V *vs* Ag/AgCl)[12] with OER. Measuring the CVs of the other used ligands was not possible due to their poor solubility in water. CVs of the electrolytes were also measured and are presented in the ESI. The electrolytes have some rising current as more positive potential values are approached, since we are reaching the instability of water in those potentials. Therefore, the OER and instability of the aqueous solution can cause some possible deviation to the results by affecting the baseline of some of these complexes (the experimental CVs with the simulated CVs are presented in ESI). [Fe(II)(D (OMe)-bpy)_3]^{2+} complex does not have a flat baseline in the CVs and therefore the fitting of this complex is not as accurate as for the ones with a flat baseline.

Relative standard deviations (RSD) are reported for the digitally extracted values in Table 2 and Table 3 to help understand the statistical significance of these results. k^0 is a sensitive value and even large changes in k^0 between different scan rates do not necessarily have influence on the CV with such small values we are dealing with. D is not as sensitive as k^0 but is affected by the baseline of the electrolyte. Its RSD values are rather sensible. RSD for k_c values seem rather large for some complexes, but we need to keep in mind that the k_c is a time-dependent variable. We are using 10–200 mV/s scan rates and the 10 mV/s might have significantly larger values for chemical reaction due to larger time for the chemical reaction to occur, and hence larger effect on the reduction current. This leads to a larger deviation between the samples. The sensitivity of the parameters is demonstrated in the ESI for the addition to the SD calculations.

3.2.1. Charge transfer coefficient α and diffusion coefficient D

The experimental voltammetry curves were reproduced successfully with simulations where the charge transfer coefficient α was set to 0.5 for all but one of the samples, indicating that a symmetric energy barrier is likely for all the measured complexes. The diffusion coefficients obtained for the unsubstituted $[Fe(II)(bpy)_3]^{2+}$ complexes with different counterions in 0.1 M phosphate buffer (pH 7) have similar values with each other and with the literature[22]. In literature the D of $[Fe(II)(bpy)_3]SO_4$ has been reported to be $1.6–2.1 \times 10^{-6}$ cm^2/s in 1 M 2-propanol and 1 M NaCl, and in 1 M NaCl respectively.[22] Other samples showed deviations for diffusion coefficients in phosphate buffer within the complexes with different counterions, indicating that the counterion affects the diffusion of the Fe(II) complexes at the electrode surface, likely due to ion pair formation. For Fe(II) complexes with sulfate counterions the diffusion coefficients were found to be significantly higher in the other electrolytes used in the study, compared to the values obtained for the same complex in phosphate buffer. In general, the smallest complex of $[Fe(II)(bpy)_3]^{2+}$ without sidegroups had the highest diffusion coefficients, regardless of the counterion or the electrolyte. The value of D is expected to decrease when the size of the sidegroup and therefore the complex increases, but there are outliers from that trend. If we look at the different electrolyte tests for complexes with sulfate

counterion (Table 3), we can see the trend between the size of the complex and the diffusion coefficient, if the values for methylated Fe(II) complex are disregarded. Most variation in the diffusion coefficient values can be seen within $[Fe(II)(bpy)_3]^{2+}$ in different electrolytes.

3.2.2. Standard rate constant k^0

The counterion present in the solid material seems to affect the standard rate constant k^0. When sulfate is used as the counterion for different iron complexes in phosphate buffer, the rate constants are nearly similar. Then again for complexes with tetrafluoroborate as the counterion, the k^0 value decreases with the increasing size of the substituent, indicating a slower redox reaction with the increasing size of the complex. However, the variation is within the sensitivity of the method, so these effects should be verified with more accurate methods such as rotating disk electrode studies.

$[Fe(II)(bpy)_3]^{2+}$ complex with the electron donating sidegroups (Me, *t*Bu and OMe) and the non-substituted $[Fe(II)(bpy)_3]^{2+}$ have in general higher rate constant k^0 for the oxidation reaction than $[Fe(II)(bpy)_3]^{2+}$ complex with electron-withdrawing groups (COO$^-$). The standard rate constant k^0 can be significantly increased, almost quadrupled, by replacing phosphate buffer with another electrolyte. Thus, some electrolyte ions (depending on the respective complex) have an enhancing effect on the redox reaction. It may be that the ability of the counter ions to stabilize the transition states of the complex during the redox reaction varies. It is also well known that the kinetics of electron transfer can be influenced by cations too[24]. Nevertheless, as the complexes under study are positively charged, anions are assumed to contribute more to the stability of the complex in different redox states than cations.

3.2.3. Rate for the chemical reaction k_c

The CVs of all samples show a typical response of an EC reaction, i.e. the reduction peak current on the return sweep is smaller than would be for a reversible redox reaction. Therefore, oxidation of the complex is followed by decomposition of the complex, as explained above. As the ligands have typically poor solubility in water, the detached ligands can precipitate, partially blocking the surface of the working electrode. The reduced WE surface area may result in a misleading decrease in the determined diffusion coefficient values. When comparing the simulated diffusion coefficient and chemical reaction rate values of Fe(II) complexes with sulfate counterions in different electrolytes, a higher diffusion coefficient value correlated with the lower chemical reaction rate of the oxidized species indicating reduced WE surface area.

The lowest rate for the chemical reaction was obtained for $[Fe(II)(DMe-bpy)_3]^{2+}$ with both sulfate and tetrafluoroborate counterions in all electrolytes indicating that the methyl group in the ligand structure decreases rate of the decomposition of the Fe(III) species. On the other side of this scale, $Na_{4+x}[Fe(II)(Dcbpy)_3](BF_4)_x$ in phosphate buffer had the highest rate for the chemical reaction, although the analysis of the voltammetry was complicated due to the concurrent oxygen evolution and/or bipyridine ligand oxidation reaction. The extracted value of k_c increases tenfold when the scan rate is increased from 10 mV/s to 200 mV/s. The experimental CVs could be fitted only with a low charge transfer coefficient of 0.3 for this complex in phosphate buffer. Thus, the energy barrier is not symmetric for the $Na_{4+x}[Fe(II)(Dcbpy)_3](BF_4)_x$ complex, and the oxidation reaction is favored over reduction. The rate constant for the electrochemical reaction k^0 is also the lowest of the measured complexes. As these results differed with the results obtained in 0.5 M NaCl by Li *et al.*[12], the measurements were repeated at pH 4 in a phthalate buffer. All the extracted values for the complex in question are better in pH 4 compared to the ones in phosphate buffer pH 7: k^0 is 9 times higher, D is increased by 50 %, α can be taken as 0.5 and the rate of the chemical reaction k_c is comparable to the iron complexes with sulfate ions as counterions. The CV data reported by Li *et al.*[12] was also analyzed by simulation, indicating absence of a following chemical reaction. The difference regarding the presence of a chemical reaction might be explained by availability of BF_4^- from the NaBF$_4$ salt shown by

^{19}F NMR (ESI). BF_4^- ions might be forming adducts with the bipyridine ligand, resulting in faster decomplexation.[25] We were able to tune the k_c value of our $Na_{4+x}[Fe(II)(Dcbpy)_3](BF_4)_x$ by changing the pH of the electrolyte from 7 to 4, which decreases rate of the decomposition of the Fe(III) complex.

Fe complexes with sulfate as the counterion have clearly lower k_c value than the same complexes with tetrafluoroborate counterions, both in phosphate buffer. Thus, the counterion used in the synthesis of the complex correlates in some way with the rate of the decomposition of the Fe^{3+} species. The counterion concentration (sulfate 0.5 mM, tetrafluoroborate 1 mM) is relatively low compared to the concentration of the phosphate buffer (100 mM), containing HPO_4^{2-} and $H_2PO_4^-$ at pH 7. The clear differences observed between tetrafluoroborate and sulfate counterions are therefore surprising. One possible explanation is that the BF_4^- ions hydrolyze readily in aqueous conditions and ions may react with nitrogens in the bpy ligand, forming $bpy(BF_3)_2$ and accelerating the decomplexation.[25] This could explain the higher k_c values in sample solutions with tetrafluoroborate counterions compared to sulfate counterions. Hydrolyzation of BF_4^- has been reported[21] to occur with similar iron complexes than used here with tetrafluoroborate counterions in the electrolyte. Therefore, the electrochemical parameters measured with sulfate counterion are more reliable.

3.3. Solubility and stability

3.3.1. Solubility and stability in 0.1 M phosphate buffer pH 7

All iron complexes were dissolved and characterized electrochemically in 0.1 M phosphate buffer at pH 7. The stabilities of these sample solutions were observed during the CV measurements and over time. The relative stabilities of the Fe^{3+}/Fe^{2+} complexes are summarized in Fig. 3. Sample decomposition in phosphate buffer was observed via a color change in the solution from different shades of red and dark red to a less intense red/colorless solution with solid precipitates forming over time. Used ligands are not typically water-soluble and they appear as white solids in the solutions after decomplexation. All sample solutions in phosphate buffer accumulated small amounts of white solids over time, while some samples started decomposing immediately after dissolving the iron complex in the phosphate buffer solution. $[Fe(II)(D(CO_2Me)\text{-}bpy)_3](BF_4)_2$, $[Fe(II)(bpz)_3](BF_4)_2$ and $[Fe(II)(DBr\text{-}bpy)_3](BF_4)_2$ showed fast decomposition in the solution. $[Fe(II)(DBr\text{-}bpy)_3](BF_4)_2$ solution decomposed quickest to form white solids and lost red color within minutes. $[Fe(II)(bpz)_3](BF_4)_2$ lost its red color soon after dissolving and was almost colorless within 30 min from preparing the solution. $[Fe(II)(D(CO_2Me)\text{-}bpy)_3](BF_4)_2$ started showing solid formation in phosphate buffer during electrochemical CV measurements, which was well visible approximately 1 h after dissolving. $[Fe(II)(DtBu\text{-}bpy)_3]SO_4$ (1 mM) showed white precipitation during electrochemical

measurement, but a decrease of concentration down to 0.5 mM reduced precipitation. $[Fe(II)(DtBu\text{-}bpy)_3](BF_4)_2$ did not dissolve properly and decomposition was rather quick.

Further comparison of the stability of the studied complexes shows, that $[Fe(II)(bpy)_3]^{2+}$ with both counterions, $[Fe(II)(DMe\text{-}bpy)_3]$ with both counterions and $Na_{4+x}[Fe(II)(Dcbpy)_3](BF_4)_x$ were the most stable complexes in phosphate buffer. They showed the least solid formation over time compared to the other samples and maintained the red color of the solution even after several months, indicating the stability of Fe^{2+} species. This stability is demonstrated in Fig. 3 by estimating the decomposition ratios for the studied complexes based on the observations of their color change and solid formation in time. The compounds can be divided into three different categories: 1) unstable, 2) stable for the duration of the measurements, and 3) relatively stable for weeks. These stabilities of Fe^{2+} complexes are presented in Fig. 3, together with the stability of the Fe^{3+} species. Comparison of the relative stabilities of the Fe^{2+} species is rather arbitrary and could be carried out more quantitatively, for example by following the UV/Vis spectra during storage. However, this rough comparison is helpful for general evaluation, as well as for the purpose of this study since all studied Fe species seem to be too unstable for flow battery applications. The stability of Fe^{3+} species is presented with the reciprocal of the rate constant for the chemical reaction occurring for the oxidized species extracted from digital simulations.

As we can see from Fig. 3, the counterions do not affect the stability of the Fe^{2+} species but they influence the stability of Fe^{3+}. Also the substituent effect is clear. Sidegroups of Me and Dc alongside the non-substituted $[Fe(II)(bpy)_3]^{2+}$ seem to result in rather stable Fe^{2+} species while substituents such as OMe and tBu lead to less stable Fe^{2+} species. Substituents of Br and CO_2Me in bpy, and bpz complex showed the quickest decomposition in solution, indicating the most unstable Fe^{2+} of the studied complexes. Complexes having both relatively good stabilities of Fe^{3+} and Fe^{2+} species were $Na_{4+x}[Fe(II)(Dcbpy)_3](BF_4)_x$ in pH 4 phthalate buffer and Me substituted $[Fe(II)(bpy)_3]^{2+}$ with sulfate ion in phosphate pH 7 buffer.

$[Fe(II)(bpy)_3]^{2+}$ with both counterions, $[Fe(II)(DMe\text{-}bpy)_3]^{2+}$ with both counterions and $Na_{4+x}[Fe(II)(Dcbpy)_3](BF_4)_x$ complexes were also tested in 1 M KOH. $Na_{4+x}[Fe(II)(Dcbpy)_3](BF_4)_x$ was further investigated in 0.5 M NaCl, in 0.5 M NaCl and HCl mixture (pH 2.4) and in phthalate buffer (pH 4). The complex was soluble in 0.5 M NaCl solution and in pH 4, but not that well in pH 2.4. It was most stable at pH 4, though a small amount of white solids was visible in the vial after one day. Stabilities of the 0.5 mM solutions of $[Fe(II)(bpy)_3]SO_4$, $[Fe(II)(DMe\text{-}bpy)_3]SO_4$ and $[Fe(II)(DtBu\text{-}bpy)_3]SO_4$ complexes in 1 M sulfuric acid were observed during and after the CV measurements. Acidic and basic conditions promoted the complex decomposition compared to neutral pH. In 1 M KOH, the solutions changed from a red liquid to a
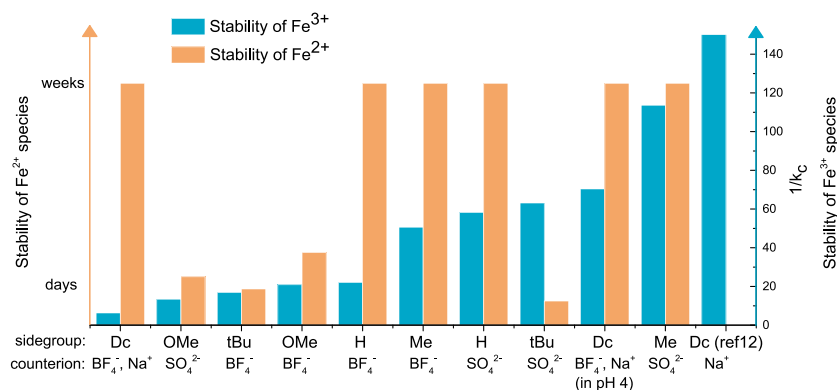

Fig. 3. Stability of $[Fe(II)(bpy)_3]^{2+}$ with different sidegroups and counterions presented by the estimated ratio of decomposition over time. The stability of Fe^{3+} species is presented by $1/k_c$. Hence, the higher bar indicates better stability for both Fe species. The electrolyte was 0.1 M phosphate buffer pH 7. More information in ESI.

colorless clear liquid with an orange precipitate, most likely Fe(III)hydroxide salt according to the Pourbaix diagram of Fe. In 1 M sulfuric acid, [Fe(II)(bpy)$_3$]SO$_4$ and [Fe(II)(DMe-bpy)$_3$]SO$_4$ turned from red solution to colorless. [Fe(II)(DtBu-bpy)$_3$]SO$_4$ didn't dissolve properly into the sulfuric acid solution at any point but instead dispersed as fine solids. The sample solution turned quickly to colorless. Out of these three electrolytes (1 M KOH, 1 M H$_2$SO$_4$ and 0.1 M phosphate buffer), the phosphate buffer stabilized the studied complexes best, even if not completely.

As the analysis of the voltammograms indicates, the selection of the counterion has an influence on the chemical stability of the Fe(III) species in the solution. Counterion must be chosen so that it ensures a stable complex with good solubility, as the interaction between the complex and the counterions in the solid state reduces solubility. Tetrafluoroborate ions should be avoided in aqueous solutions to hinder the decomposition of the oxidized species. According to the Pourbaix diagram of pure iron, Fe^{3+} is usually stable as an ion in acidic (pH < 4) solutions, whereas Fe^{2+} has a wider stability window from acidic to neutral pH. The observed white solid precipitates in the studied samples are expected to be ligands dissociating from the complex mixed with Fe oxides, which are usually decomposition products in Fe solutions in aqueous near neutral pH solutions. Thus, modifying the structure of the iron complex with acidic groups, such as COOH, or optimizing the pH and the composition of the electrolyte, would be good options for stabilizing the redox species further, and minimizing the chemical decomposition reactions happening in the solution. Considering all this, the stability of the iron complexes with sulfate counterions were chosen for further study in different aqueous electrolytes.

3.3.2. Solubility and stability in 0.1 M KNO$_3$, 0.1 M K$_2$SO$_4$ and 0.1 M NaCl solutions

Fe(II) complexes with sulfate counterions were dissolved and characterized via cyclic voltammetry also in 0.1 M KNO$_3$, 0.1 M K$_2$SO$_4$ and 0.1 M NaCl. Stabilities of these iron complex solutions were observed during CV measurements and over time similarly than samples in phosphate buffer. Solubility of Fe(II) complexes with sulfate ions in all mentioned solutions was good in the applied concentration of 0.5 mM except for [Fe(II)(DtBu-bpy)$_3$]SO$_4$ in 0.1 M KNO$_3$. The last-mentioned sample was a blurry red solution while dissolving and turned into a bulkier reddish solid at the bottom of the vial in the next day. All other samples were considered stable during the measurements: no solid precipitate formation or de-coloring of the solutions took place. The relative stabilities of Fe^{2+} complexes in the solutions were generally evaluated as mentioned for the Fe complexes in phosphate buffer. However, the stability of Fe^{2+} complex is marked by the first precipitate formation over time, since the complexes seemed to keep their red color for a long time and were considered stable in terms of color change. In Fig. 4., the stability of Fe^{2+} complex is presented as estimated relative stability considering the time of the first solid formation in the solution,

and the stability of Fe^{3+} species is presented as reciprocal of the rate constant for the decomposition reaction k_c taking place for the oxidized species.

[Fe(II)(DMe-bpy)$_3$]SO$_4$ in 0.1 M KNO$_3$, 0.1 M K$_2$SO$_4$ and 0.1 M NaCl along with the [Fe(II)(D(OMe)-bpy)$_3$]SO$_4$ in 0.1 M NaCl seem to have the most stable reduced species of the mentioned solutions regarding solid formation. Generally, NaCl and KNO$_3$ seem to be the best electrolytes regarding the stability of Fe^{2+} species, but there is some deviation between iron complexes with different side groups. However, intense red color is maintained in every solution included in Fig. 4 even after several weeks, indicating that the Fe^{2+} complex is rather stable in these aqueous electrolytes. The least amount of solid formation was found in the [Fe(II)(DMe-bpy)$_3$]SO$_4$ solutions that remained solid-free longer than other sample solutions, indicating that methylation hinders the decomposition of Fe^{2+} species. However, all the Fe complex solutions under inspection here had a very small amount of solid formation.

3.4. Battery testing

Based on the performed simulations, the most stable Fe(II) complex is [Fe(II)(DMe-bpy)$_3$]SO$_4$. The best electrolyte for it is 0.1 M K$_2$SO$_4$ when comparing the rates for the chemical reaction of the oxidized species. Since precipitate formation of the Fe(II) species may be influenced by exposure to air, it was not considered as a criterion when choosing the electrolyte for further battery testing in an oxygen-free glovebox.

[Fe(II)(DMe-bpy)$_3$]SO$_4$ was studied as a posolyte (2 mM) versus 4 mM NDI as a negolyte in an asymmetric lab-scale flow battery by utilizing galvanostatic cycling. The used electrolyte was 0.1 M K$_2$SO$_4$. The same complex was studied in a symmetric cell versus oxidized [Fe(II)(DMe-bpy)$_3$]SO$_4$ in the same supporting electrolyte. The battery setup is presented in Fig. 5. Results of the asymmetric cell can be seen in Fig. 6 and of the symmetric cell in Fig. 7.

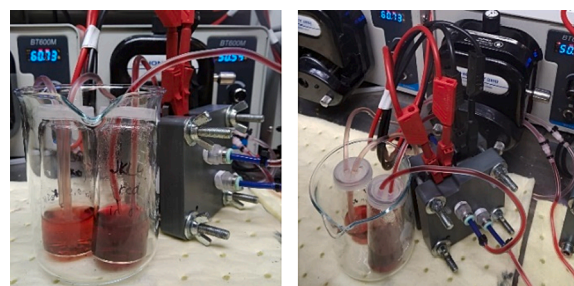Fig. 6. shows the shape of the charge–discharge cycles during battery

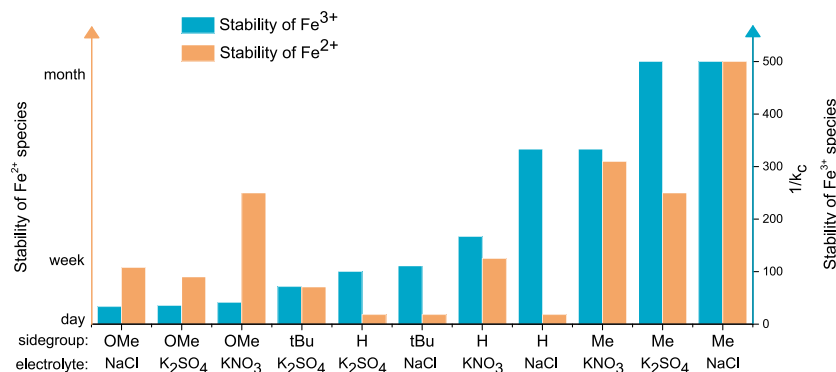**Fig. 5.** Experimental battery set-up for a symmetric battery.

Fig. 4. Stability of [Fe(II)(bpy)$_3$]$^{2+}$ with sulfate counterion and with different sidegroups by the ratio of solid formation over time, and stability of Fe^{3+} species by 1/k_c, presented in different electrolytes. The higher bar indicates better stability for both Fe species. More information on ESI.
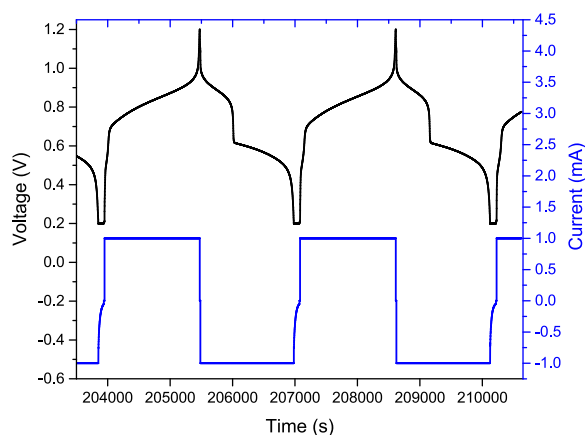
Fig. 6. The shape of the charge/discharge curve showing dimer formation during asymmetric battery cycling with $[Fe(II)(DMe-bpy)_3]^{2+}$ as posolyte and NDI in excess as negolyte, the electrolyte for both was 0.1 M K_2SO_4. The battery was charged/discharged with constant current (1 mA) until the voltage was 1.2 V or 0.2 V respectively. The constant current step was followed by a constant voltage step with mentioned voltages until the current was less than 0.01 mA to achieve full charge/discharge.

cycling for the asymmetric battery cell. We observe one plateau during charging (oxidizing the Fe(II) complex to Fe(III)) and two plateaus during discharge (reduction of Fe(III) to Fe(II) species). This shape indicates dimer formation as this behavior has been recently reported[20] for a non-substituted $[Fe(II)(bpy)_3]^{2+}$ by Holubowitch and Nguyen. In their work, the dimer formation with an oxo-bridge between two oxidized Fe(III) monomer centers was described and related to a similar charge/discharge shape of the compound as the shape of our battery results. This indicates that our charge plateau is related to monomer oxidation. The two discharge plateaus are due to the discharge of the monomer and dimer: the plateau with the higher potential is related to the discharge of the monomer and the lower plateau is due to the discharge of the dimer The observed dimer formation with an oxo-bridge between two Fe centers of $[Fe(III)(DMe-bpy)_3]^{3+}$ is a rather reversible process, leading to two Fe(II) monomers upon discharge. This seems to be a rather reversible process, since most of the monomer is present after the dimer discharging and can be oxidized again in the next cycle. However, the energy efficiency of this process is not good due to the voltage drop between the monomer and the dimer discharge plateaus. This means some of the energy that is charged to the monomer is

lost to the dimer formation and that energy cannot be discharged back from the dimer. The ways to block this possible dimer formation were not studied, but must be considered in the further design work of Fe(II) complexes.

Fig. 7. A) shows the shape of the charge–discharge curve of the symmetric cell with $[Fe(II)(DMe-bpy)_3]^{2+}$ as posolyte and $[Fe(III)(DMe-bpy)_3]^{3+}$ as negolyte, both approximately 2 mM in 0.1 M K_2SO_4. Some material has been lost to the carbon felts (observed as reddish orange solids after the cycling) and to the membrane by aggregation, meaning that the real concentration is lower. The negolyte was prepared by oxidizing the Fe(II) species in another battery before the symmetric cell assembly, leading to some loss of the material. The small concentration of the redox species (2 mM) is therefore making the comparison of the charge/discharge capacity with the theoretical one (approximately 0.8 mAh) tricky. The shape of the charge/discharge curve changes from the first to the last cycle. The plateaus related to the discharge of the dimer are becoming more visible, and vice versa, the plateaus related to the monomer charge/discharge processes seem to diminish. This indicates dimer becomes dominant compared to the monomer species in both the negolyte and the posolyte. However, these solutions were not characterized after the battery testing, and conclusions relating to the dimer formation are based on the literature[20] on dimer formation of non-substituted $[Fe(III)(bpy)_3]^{3+}$.

The theoretical capacity corresponding to 2 mM concentration of both redox species is 0.80 mAh. However, some imbalance might occur between the solutions, since the negolyte had been oxidized in another battery and some material may be lost in transfer to the symmetric battery. The best capacity in the symmetric battery test was at the beginning of the measurements 0.63 mAh, which is 78 % of the theoretical capacity. In every cycle, charging of the battery required more energy than what was regained in the discharge, resulting in a capacity decay of 0.35 % per cycle within the first 79 cycles. All in all, the capacity decay in the symmetric battery leads to the conclusion that the $[Fe(II)(DMe-bpy)_3]^{2+}/[Fe(III)(DMe-bpy)_3]^{3+}$ is not stable. Dimer formation decreases the energy capacity and the voltage drop caused by dimer formation of Fe(III) species lowers the energy efficiency, resulting in lost energy due to dimer formation upon discharge. Also, the monomer recovery from the dimer does not seem to be fully reversible.

4. Conclusions

The formal potentials of the $[Fe(II)(bpy)_3]^{2+}$ complexes can be adjusted by selecting different sidegroups to bpy. Adding electron-withdrawing groups, such as in dicarboxyl functionalized iron(II)
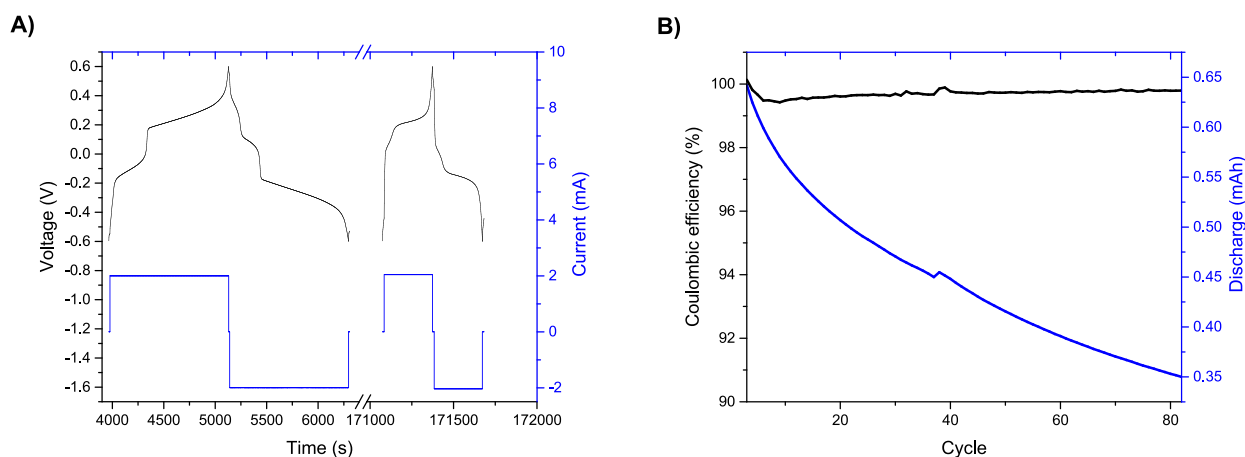

Fig. 7. A) Changes in the shape of the charge/discharge curve at the beginning and at the end of the galvanostatic cycling in a symmetric battery with $[Fe(II)(DMe-bpy)_3]^{2+}$ as posolyte and $[Fe(III)(DMe-bpy)_3]^{3+}$ as negolyte during almost 300 cycles. Plateaus related to monomer seem to be shrinking with increasing cycle numbers and dimer charge/discharge seem to become more dominant. Charged/discharged energy is also decaying as indicated by shorter plateaus at the end of cycling. B) Capacity decay of the symmetric battery set-up for discharge energy with stable Coulombic efficiency.

bipyridine, shifts the formal potential to the positive direction from [Fe (II)(bpy)$_3$]$^{2+}$ (E^0 0.875 V *vs.* Ag/AgCl) resulting in an E^0 value of 0.97 V *vs.* Ag/AgCl. Adding electron-donating groups shifts the formal potential of the complex to the negative direction from [Fe(II)(bpy)$_3$]$^{2+}$ resulting in the lowest measured E^0 of 0.56 V for dioxymethyl functionalized bipyridine complex.

Selection of the counterion affects the solubility of the complex but also the rate of the chemical reaction of the Fe(III) species and therefore the chemical stability of the oxidized form of the complex. The rates of following chemical reactions can be extracted from voltammetry analysed by digital simulations. Dimethyl functionalized bipyridine complex showed the lowest rates for the chemical reaction of Fe^{3+} in 0.1 M KNO$_3$, 0.1 M K$_2$SO$_4$ and 0.1 M NaCl. Also [Fe(III)(bpy)$_3$]$^{3+}$ had a very low decomposition rate in 0.1 M NaCl.

Stability of Fe^{2+} complex was good in 0.1 M phosphate buffer pH = 7 for tris bipyridine and for both dimethyl functionalized and dicarboxyl functionalized bipyridines, with the red colour of the solutions maintained even after several months and where only small amount of solids was observed. Stabilities of the Fe^{2+} complexes prepared as sulfate salts were good also in 0.1 M KNO$_3$, 0.1 M K$_2$SO$_4$ and 0.1 M NaCl, with the tiny solid formation and intense red color even after several weeks. Most stable of the studied complexes considering both the stability of Fe^{2+} and Fe^{3+} species was dimethyl functionalized bipyridine complex. The presence of even small amounts of tetrafluoroborate was observed to increase the rate of the chemical reaction of the Fe(III) complex, and should therefore be avoided for aqueous electrolytes.

Asymmetric battery testing of the dimethyl functionalized bipyridine complex indicated dimer formation as the decomposition mechanism observed in the voltammetry experiments. Dimer formation is expected to happen in our battery due to the similar shape of the charge–discharge curve with the dimer discharging at a lower potential than the monomer, as recently reported in the literature[20] for [Fe(II) (bpy)$_3$]$^{2+}$ complexes. This voltage drop is disadvantageous, as it decreases the voltage efficiency of the battery. Capacity decay was also detectable, at the rate of 0.35 % per cycle during 79 cycles, indicating that the monomer cannot be recovered totally from the dimer discharge.

The studied complexes were not sufficiently stable and hence not suitable for aqueous flow battery applications. Nevertheless, qualitative information on reasons for the decomplexation and solubilities, as well as information on the substituent effect on these and the formal potential, are important in developing suitable metal complexes for flow battery applications in water solutions. Voltammetry coupled with digital simulations was demonstrated to be an excellent tool for initial evaluation of the stabilities of the oxidized forms. Further development of these complexes by finding a way to block the dimer formation would lead to a better energy efficiency and possibly to a better stability in battery cycling, achieved for example with an asymmetric ligand design.

CRediT authorship contribution statement

Jenna Hannonen: Investigation, Formal analysis, Validation, Writing – original draft. **Anniina Kiesilä:** Investigation, Formal analysis, Validation, Writing – original draft. **Ulriika Mattinen:** Writing – review & editing. **Petri M. Pihko:** Funding acquisition, Conceptualization, Supervision, Writing – review & editing. **Pekka Peljo:** Funding acquisition, Conceptualization, Supervision, Methodology, Validation, Writing – review & editing.

Declaration of Competing Interest

The authors declare that they have no known competing financial interests or personal relationships that could have appeared to influence the work reported in this paper.

Acknowledgements

Appendix A. Supplementary data

Supplementary data to this article can be found online at https://doi.org/10.1016/j.jelechem.2023.117847.

References

[1] F. Blau, Ber. Dtsch. Chem. Ges. 21 (1888) 1077–1078.
[2] C. Kaes, A. Katz, M.W. Hosseini, Chem. Rev. 100 (2000) 3553–3590.
[3] F. Blau, Monatsh. Chem. 19 (1898) 647–689.
[4] L.P. Hammett, G.H. Walden, R.P. Chapman, J. Am. Chem. Soc. 53 (1931) 3908.
[5] Y. Matsuda, K. Tanaka, M. Okada, Y. Takasu, M. Morita, T. Matsumura-Inoue, J. Appl. Electrochem. 18 (1988) 909–914.
[6] C. Yang, G. Nikiforidis, J.Y. Park, J. Choi, Y. Luo, L. Zhang, S.C. Wang, Y.T. Chan, J. Lim, Z. Hou, M.H. Baik, Y. Lee, H.R. Byon, Adv. Energy Mater. 8 (2018) 1–10.
[7] J. Mun, M.J. Lee, J.W. Park, D.J. Oh, D.Y. Lee, S.G. Doo, Electrochem. Solid-State Lett. 15 (2012) A80–A82.
[8] J. Mun, D.-J. Oh, M.S. Park, O. Kwon, H.-T. Kim, S. Jeong, Y.G. Kim, M.-J. Lee, J. Electrochem. Soc. 165 (2018) A215–A219.
[9] X. Xing, D. Zhang, Y. Li, J. Power Sources 279 (2015) 205–209.
[10] X. Xing, Y. Zhao, Y. Li, J. Power Sources 293 (2015) 778–783.
[11] P. Vanýsek, Electrochemical Series, in: W.M. Haynes (Ed.), Handbook of Chemistry and Physics, 93rd ed., CRC Press, 2012.
[12] X. Li, P. Gao, Y.Y. Lai, J.D. Bazak, A. Hollas, H.Y. Lin, V. Murugesan, S. Zhang, C. F. Cheng, W.Y. Tung, Y.T. Lai, R. Feng, J. Wang, C.L. Wang, W. Wang, Y. Zhu, Nat. Energy 6 (2021) 873–881.
[13] T. Carnelley, Lond. Edinb. Dubl. Phil. Mag. 13 (1882) 180–193.
[14] A.J. Bard, L.R. Faulkner, Electrochemical Methods: Fundamentals and Applications, 2nd Edition, John Wiley & Sons Inc., 2001.
[15] J. Gao, K. Amini, T.Y. George, Y. Jing, T. Tsukamoto, D. Xi, R.G. Gordon, M.J. Aziz, Adv. Energy Mater. 12 (2022) 2202444.
[16] H.E. Gottlieb, V. Kotlyar, A. Nudelman, J. Org. Chem. 62 (1997) 7512–7515.
[17] L. Patiny, A. Borel, J. Chem. Inf. Model. 53 (2013) 1223–1228.
[18] C. Wiberg, L. Evenäs, M. Busch, E. Ahlberg, J. Electroanal. Chem. 896 (2021), 115224.
[19] Y.-W.-D. Chen, K.S.V. Santhanam, A.J. Bard, J. Electrochem. Soc. 128 (1981) 1460–1467.
[20] N.E. Holubowitch, G. Nguyen, Inorg. Chem. 61 (2022) 9541–9556.
[21] C.X. Cammack, H.D. Pratt, L.J. Small, T.M. Anderson, Dalton Trans. 50 (2021) 858–868.
[22] H. Bui, N.E. Holubowitch, Int. J. Energy Res. 46 (2022) 5864–5875.
[23] H. Ferreira, K.G. von Eschwege, J. Conradie, Electrochim. Acta 216 (2016) 339–346.
[24] J. Kuta, E. Yeager, J. Electroanal. Chem. Interfac. Electrochem. 59 (1975) 110–112.
[25] E.V. Carino, C.E. Diesendruck, J.S. Moore, L.A. Curtiss, R.S. Assary, F.R. Brushett, RSC Adv. 5 (2015) 18822–18831.